

Study On Multiscale-Multivariate Attribution Analysis and Prediction of Urban Rainstorm Flood

Jinping Zhang

Zhengzhou University

Yuhao Wang (✉ 731270945@qq.com)

Zhengzhou University

Research Article

Keywords: Urban rainstorm flood, Multiscale attribution analysis, Flood prediction, Wavelet analysis method, Ridge regression model

Posted Date: November 16th, 2021

DOI: <https://doi.org/10.21203/rs.3.rs-929111/v1>

License: © ⓘ This work is licensed under a Creative Commons Attribution 4.0 International License.

[Read Full License](#)

1 **Study on Multiscale-multivariate Attribution Analysis and Prediction of Urban**

2 **Rainstorm Flood**

3 Jinping Zhang^{a,b,c}, Yuhao Wang^{a*}

4 a. *School of Water Conservancy Engineering, Zhengzhou University, Zhengzhou, 450001,*
5 *China;*

6 b. *State Key Laboratory of Severe Weather, Chinese Academy of Meteorological Sciences,*
7 *Beijing, 100000, China;*

8 c. *Yellow River Institute for Ecological Protection & Regional Coordinated Development,*
9 *Zhengzhou University, Zhengzhou, 450001, China*

10

11 **Corresponding author. Tel.: +86-17538130612*

12 *E-mail addresses: wyh19971030@163.com (Yuhao Wang)*

13

14 **Abstract:** In order to explore the impact of the changing environment on urban rainstorm flood,
15 and reveal the relationship between flood volume and its influencing factors at the micro level,
16 the rainfall and flood volume are decomposed by the wavelet analysis method to perform the
17 multiscale attribution analysis. Then the multiscale-multivariate prediction model of urban
18 rainstorm flood is constructed in the Jialu River Basin in Zhengzhou city of China. The results
19 show that the main influencing factors of flood volume are rainfall and underlying surface,
20 where the latter causes the mutation of flood volume in 1994 and 2005. At the micro level, there
21 is a constant linear relationship between rainfall and flood volume in d1, d2 and d3, while the

22 impact of underlying surface on flood volume is mainly reflected in a3. The multiscale-
23 multivariate prediction model has a good simulation effect on the flood volume of the first 45
24 rainstorm floods, NSE , R^2 and R_e are 0.966, 0.964 and 10.80%, respectively. Moreover, the
25 model also has a good prediction effect, and the relative errors between the predicted and
26 observed flood volume of 46th~50th rainstorm floods are all less than 20%.

27 **Author keywords:** Urban rainstorm flood; Multiscale attribution analysis; Flood prediction;
28 Wavelet analysis method; Ridge regression model

29 **1. Introduction**

30 For recent years, the urban rainstorm flood disaster occurs frequently causing a great threat
31 to the national economic development and people's lives and property. The continuous
32 development of urbanization will induce the continuous changes of the urban rainstorm flood
33 characteristics (Zhang et al. 2014). Therefore, many scholars have carried studies on the
34 evolution of urban rainstorm flood by constructing models such as SWMM (Wu et al. 2017;
35 Jamali et al. 2018), MIKE (Bisht et al. 2016; Li et al. 2018), InfoWorks ICM (Peng et al. 2015;
36 Gong et al. 2018;). Moreover, Nigussie et al (2019) combined MIKE 21 model with the
37 dynamic cellular automata-based urbanization model to predict urban flood under different
38 scenarios in the future. However, most studies are focused on improving rainstorm flood
39 hydrodynamic model or coupling with other methods, it is rare for the detailed study on the
40 driving factors of urban rainstorm flood evolution. Meanwhile, most of the researches focus on
41 the urban waterlogging simulation, it cannot truly reflect the overall impact of the changing
42 environment on the urban rainstorm flood, while the study on the flood process at the urban

43 river outlet can effectively solve this problem (Ren et al. 2021).

44 Nowadays, statistical model and hydrological model have been widely used for predicting
45 hydrological variables. The hydrological model works well, but it requires lots of data and is
46 complicated to operate (Yan et al. 2008; Clark et al. 2015). In contrast, the statistical model is
47 simple to operate with an acceptable prediction accuracy (Wang and Huo, 2010), so more
48 scholars have used statistical models such as linear regression model (Madarang and Kang,
49 2014; Chu et al. 2017), grey model (Ho et al. 2015; Wu and Wang, 2020) and neural network
50 model (Taormina et al. 2015; Yaseen et al. 2016) to predict hydrological variables. Moreover,
51 the statistical models are often combined with each other to improve the model performance,
52 for example, Wang et al (2019) combined the gray model with BP neural network model to
53 predict runoff and used Markov chain to correct the results. However, these statistical models
54 can not exhibit the characteristic changes of variables with the multiscales, so it also can not
55 reveal their relations between variables and their influencing factors at the micro level.

56 Obviously, the knowledge of the driving factors makes to understand the evolution law of
57 urban rainstorm flood well. Meanwhile, constructing the statistical prediction model of urban
58 rainstorm flood can quantify the relationship between flood volume and its main influencing
59 factors, thus reflect the overall impact of the changing environment on the urban rainstorm
60 flood. Moreover, it is important to predict flood volume at the macro level, but the physical
61 mechanism between flood volume and its influencing factors can be better reflected by
62 predicting flood volume at the micro level, which can be achieved by combining with wavelet
63 analysis method. Therefore, the innovation of this paper is to construct the multiscale-

64 multivariate prediction model of urban rainstorm flood by combining wavelet analysis method
65 and statistical models, thus the model can not only predict the urban flood at the macro and
66 micro levels, but also quantify the multiscale attribution characteristics of flood volume to
67 reflect the overall impact of the changing environment on urban rainstorm flood.

68 The objective of this paper is to determine the main influencing factors of flood volume
69 firstly. Secondly, the rainfall and flood volume are decomposed by the wavelet analysis method
70 to perform the multiscale attribution analysis. Thirdly, the prediction model for each flood
71 volume component is constructed, then the multiscale-multivariate prediction model of urban
72 rainstorm flood is constructed by superimposing them. Finally, the model performance
73 including simulation effect and prediction effect is evaluated.

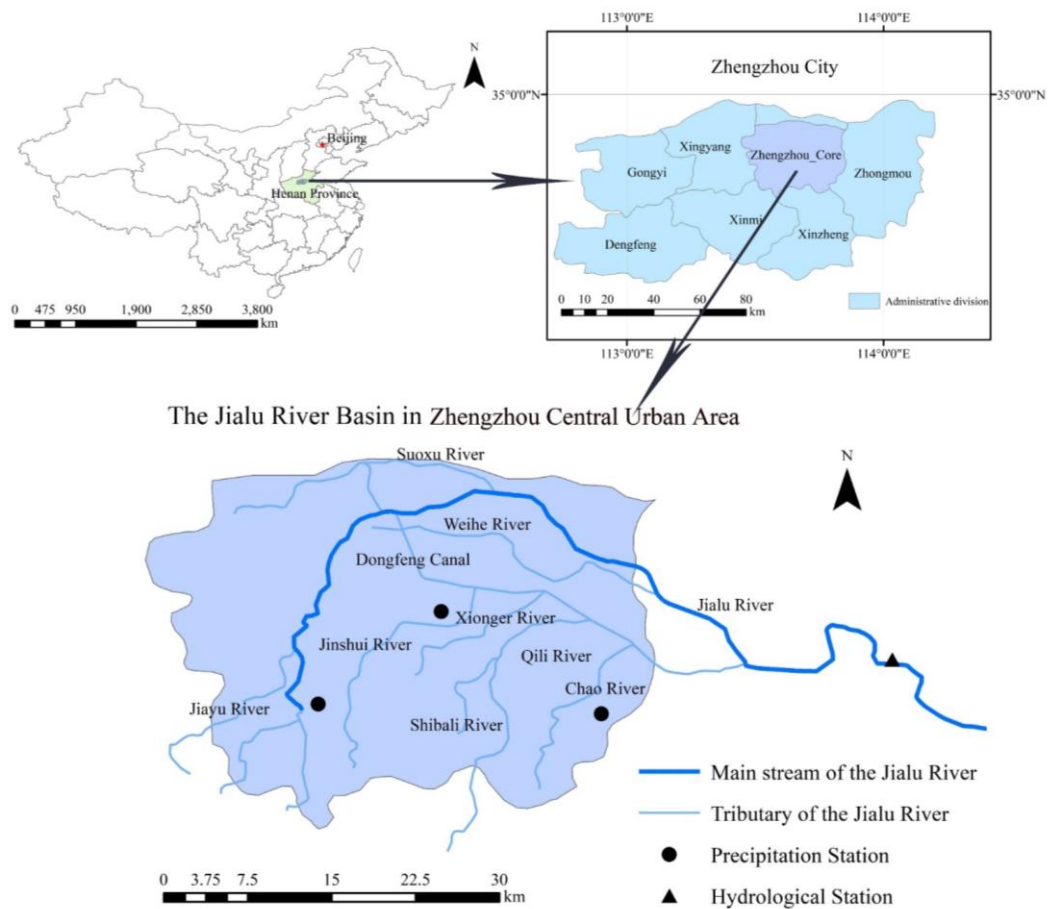
74 **2. Materials and Methods**

75 **2.1 Study Area**

76 The Jialu River originates in Xinmi City (affiliated to Zhengzhou City in China), and
77 eventually flows into the Shaying River, which is the main tributary of the Huaihe River (Sun
78 et al. 2017). The Jialu River Basin is 929 km² in Zhengzhou central urban area, accounting for
79 94% of the total area of Zhengzhou central urban area (Zhang et al. 2019).

80 In the upstream of the Jialu River, there are Changzhuang reservoir, Jiangang reservoir and
81 Hewang reservoir, thus it has no other natural water source except the main river course of Jialu
82 River. In addition, the rainwater in Zhengzhou central urban area is mainly discharged into the
83 nearby rivers, then with the Dongfeng Canal, Jinshui River, Xiong'er River, Qili River and other
84 tributaries, the rainwater flows into the Jialu River (Zhou et al. 2015). The river system map of

85 the study area is shown in Figure 1.



86

87

Figure 1. River system map of the study area

88 2.2 Data Source

89 The hourly rainfall data in this paper are from Zhengzhou Precipitation Station, Jiangang
90 Precipitation Station and Sizhao Precipitation Station, while the flood data are from Zhongmu
91 Hydrological Station. The geographical location of each station is shown in Figure 1. The
92 selected rainstorm flood must meet the following two conditions: (1) The rainfall meets the
93 standard of rainstorm magnitude in Table 1(Yang et al. 2014). For the two consecutive hours,
94 its rainfall is less than 0.1mm, thus it is considered as the end of a rainstorm (Shao et al. 2018).
95 Also, the rainfall of three precipitation stations is basically the same. (2) The flood process line

96 is a single-peak curve with a complete water recession process.

97 **Table 1. The standard of rainstorm magnitude**

Rainfall duration/h	1	2	3	6	12	24
Rainfall/mm	>15	>20	>22	>25	>30	>50

98 50 rainstorm floods are screened out from 1983 to 2018, and the corresponding rainfall is
99 the arithmetic average of the observed values at three precipitation stations. In this paper, the
100 straight-line segmentation method which connects the starting point on the rising process to the
101 turning point estimated on the recession process is used to divide flood process, and the
102 corresponding flood volume is above the connection line (Xu et al. 2011). Moreover, eight
103 phases (1980, 1990, 1995, 2000, 2005, 2010, 2015 and 2018) of the land use/cover data of study
104 area are obtained from the China Resources and Environmental Science and Data Center.

105 **2.3 Wavelet Analysis Method**

106 The basic idea of wavelet transform is to use a cluster of wavelet functions to represent or
107 approximate a certain signal or function. The corresponding wavelet function $\psi(t)$ is a function
108 having a wave shape and limited but flexible length with a mean value that is equal to zero, and
109 is localized in both time and frequency domains (Seo et al. 2015; Pathak et al. 2016). For a
110 timeseries, $\psi(t)$ is generally defined as:

$$111 \quad \psi_{a,b}(t) = |a|^{-1/2} \psi\left(\frac{t-b}{a}\right) \quad (1)$$

112 where t represents time; b is the translation factor (time shift) of the wavelet over the time series,
113 and a ranging from 0 to $+\infty$ denotes the wavelet scale (scale factor). For a given energy-limited
114 signal $f(t) \in L^2(R)$, the continuous wavelet transform (CWT) is defined as:

115
$$W_f(a, b) = |a|^{-1/2} \int f(t) \bar{\psi}\left(\frac{t-b}{a}\right) dt \quad (2)$$

116 where $\bar{\psi}\left(\frac{t-b}{a}\right)$ is the complex conjugate function of $\psi\left(\frac{t-b}{a}\right)$. In real hydrological problems,
 117 the time series are usually in the discrete format rather than continuous format (Roushangar et
 118 al. 2018), therefore, the discrete wavelet transform (DWT) in the following form is usually used:

119
$$W_f(a, b) = |a|^{-1/2} \Delta t \sum_{k=1}^N f(k\Delta t) \bar{\psi}\left(\frac{k\Delta t-b}{a}\right) \quad (3)$$

120 where Δt is the sampling interval.

121 2.4 Linear Regression Model and Ridge Regression Model

122 The core of the linear regression model is to establish a linear relationship between the
 123 dependent variable and one or more independent variables (Liu et al. 2016). When the number
 124 of independent variables is p and the number of samples is n , the linear regression model is
 125 formulated as follows:

126
$$Y = X\beta + \varepsilon \quad (4)$$

127 where $Y (n \times 1)$ is the vector of dependent variable, $X (n \times p)$ is the regression matrix, $\varepsilon (n \times 1)$
 128 is the vector of random error terms after removing the influence of independent variable on
 129 dependent variable, and $\beta (p \times 1)$ is the parameter vector which can be estimated by the least
 130 square method with the following equation (Zhao et al. 2020):

131
$$\beta = (X^T X)^{-1} X^T Y \quad (5)$$

132 When there is a good correlation between independent variables, the least squares
 133 estimator may lead to the ill-conditioned problem, that is, the calculated optimal parameter does
 134 not match the actual situation. The ridge regression model can effectively handle this problem.

135 The ridge regression is a biased estimation regression method for multicollinearity data

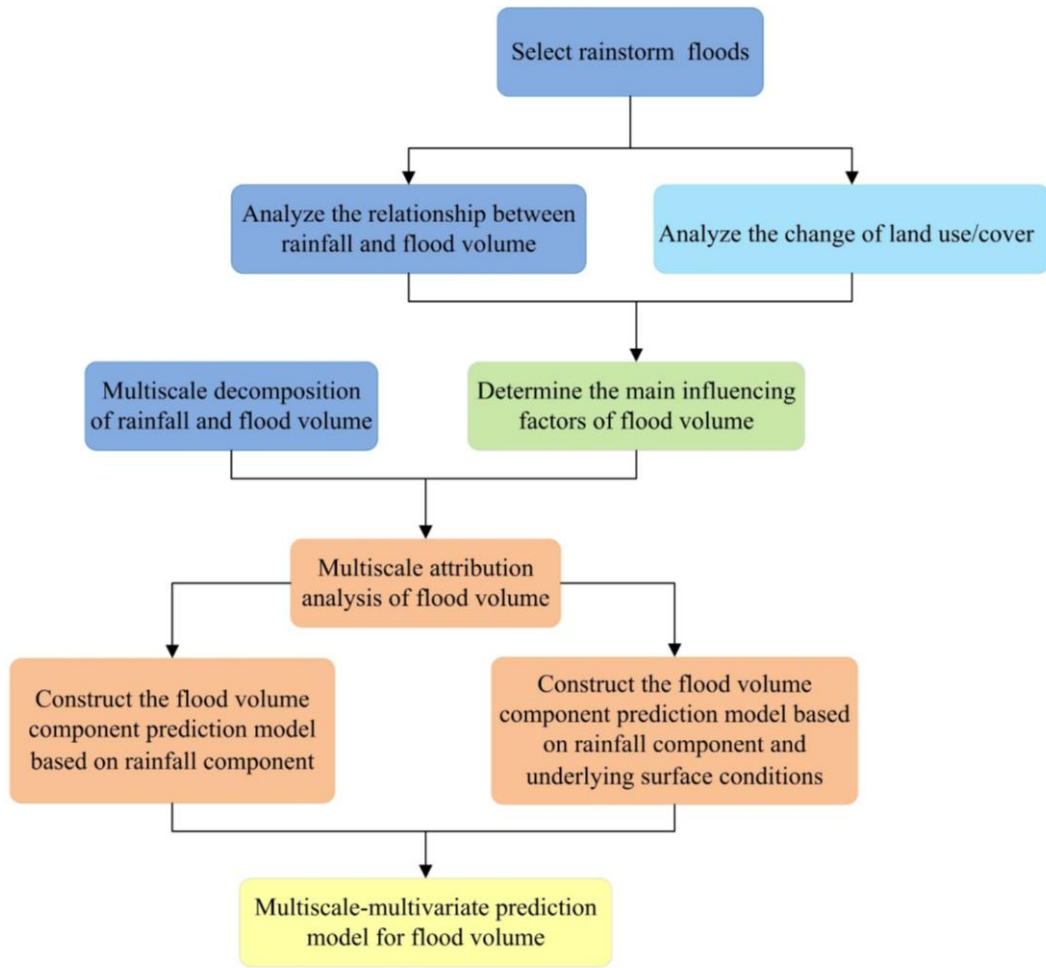
136 analysis. The motivation for the ridge estimator is to add a constant matrix kI ($k>0$) to the matrix
137 $X^T X$, which greatly reduces the probability of $X^T X + kI$ approaching singularity (Rabiei et al.
138 2019). Therefore, the parameters of the ridge regression model can be obtained with the
139 following equation:

$$140 \quad \hat{\beta} = (X^T X + kI_p)^{-1} X^T Y \quad (6)$$

141 where $k \geq 0$ is the ridge parameter and I_p is the p -dimensional identity matrix (Choi et al. 2019).

142 **2.5 Structure of the Combined Prediction Model**

143 The relationship between rainfall and flood volume is analyzed by double cumulative
144 curve method and T-test method, then the main influencing factors of flood volume can be
145 determined by combining the analysis of land use/cover change. Meanwhile, the sequences of
146 rainfall and flood volume are decomposed into several components by wavelet transform to
147 perform the multiscale attribution analysis of flood volume. According to the impact of each
148 influencing factors on the flood volume at different scales, the cumulative linear regression
149 model and ridge regression model are introduced to construct the prediction model for each
150 flood volume component. Finally, the multiscale-multivariate prediction model of urban
151 rainstorm flood is obtained by superimposing all component prediction models. The process for
152 constructing the combined prediction model is shown in Figure 2.



153

154

Figure 2. The process for constructing the combined prediction model

155

The Nash–Sutcliffe efficiency (NSE), the coefficient of determination (R^2) and the mean

156

relative error (R_e) are used to evaluate the performance of the model. The closer the values of

157

NSE and R^2 to 1.0 and the closer the value of R_e to zero, the better the performance of model

158

can be achieved. These performance indexes can be written as:

159

$$NSE = 1 - \frac{\sum_{i=1}^n (y_i - y'_i)^2}{\sum_{i=1}^n (y_i - \bar{y}_i)^2} \quad (7)$$

160

$$R^2 = \left[\frac{\sum_{i=1}^n (y_i - \bar{y}_i)(y'_i - \bar{y}'_i)}{\sqrt{\sum_{i=1}^n (y_i - \bar{y}_i)^2 \sum_{i=1}^n (y'_i - \bar{y}'_i)^2}} \right]^2 \quad (8)$$

161

$$R_e = \frac{1}{n} \sum_{i=1}^n \left| \frac{y'_i - y_i}{y_i} \right| \times 100\% \quad (9)$$

162

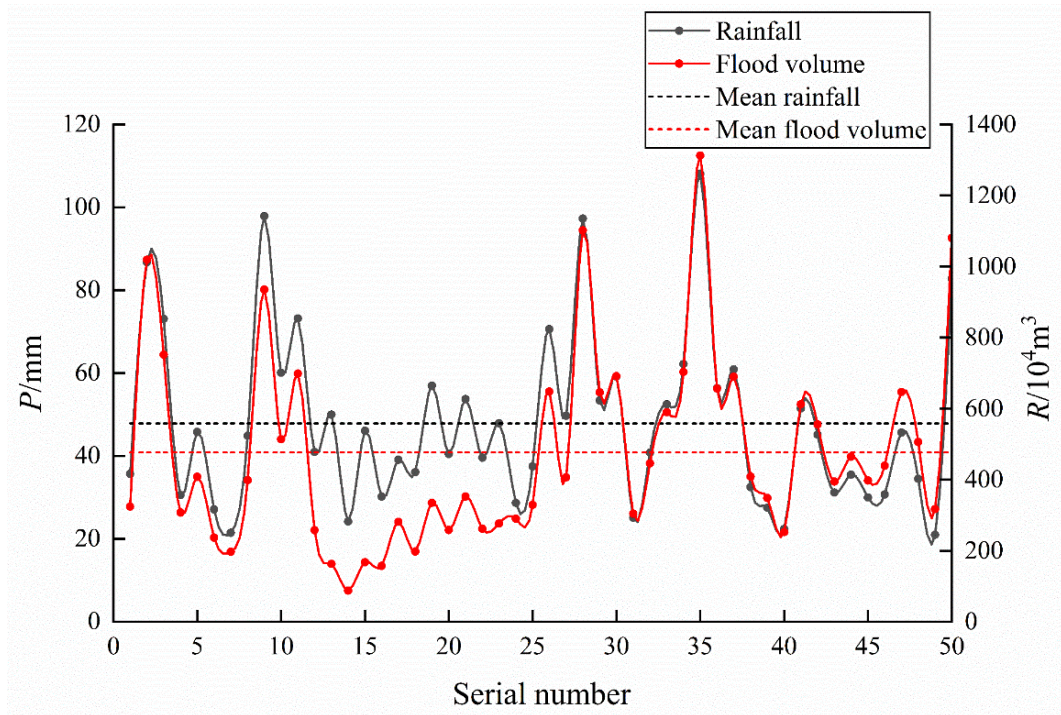
where y_i and y'_i are the i -th observed and simulated value; \bar{y}_i and \bar{y}'_i are the average

163 observed and simulated value respectively, n is the number of observations.

164 3. Results and Discussion

165 3.1 Analysis of Relationship Between Rainfall and Flood Volume

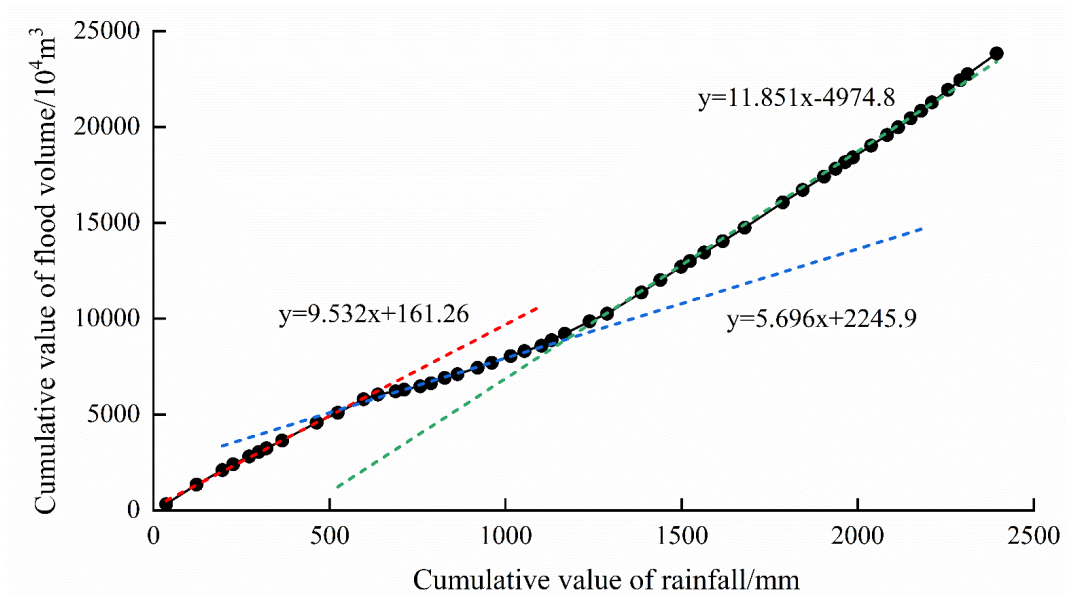
166 The rainfall and flood volume of 50 rainstorm floods are shown in Figure 3. It can be seen
167 from Figure 3 that the rainfall and flood volume of the 12th to 25th rainstorm floods are smaller,
168 while those of other rainstorm floods fluctuate around the mean value. Moreover, the fluctuation
169 trends of rainfall and flood volume are basically the same with the correlation coefficient of
170 0.876. In order to further explore the changes in the relationship between them, the double
171 cumulative curve of rainfall and flood volume is constructed as shown in Figure 4.



172

173

Figure 3. Rainfall and flood volume of 50 rainstorm floods



174

175

Figure 4. Double cumulative curve of rainfall and flood volume

176

According to Figure 4, it is obvious that the slope of the double cumulative curve changes

177

in the 12th and 24th rainstorm floods, dividing the 50 rainstorm floods into three periods

178

including the 1st rainstorm flood (September 22, 1983) ~ the 11th rainstorm flood (April 30,

179

1993), the 12th rainstorm flood (April 18, 1994) ~ the 23rd rainstorm flood (June 29, 2003),

180

the 24th rainstorm flood (June 21, 2005) ~ the 50th rainstorm flood (August 18, 2018).

181

Assuming that these two rainstorm floods are mutation points of the rainfall-flood volume

182

relationship, the significance T-test is respectively performed on the rainfall and flood volume,

183

the significance level is 0.01 and the results are shown in Table 2. If the absolute value of T

184

exceeds the critical value, it means that the significance test is passed.

185

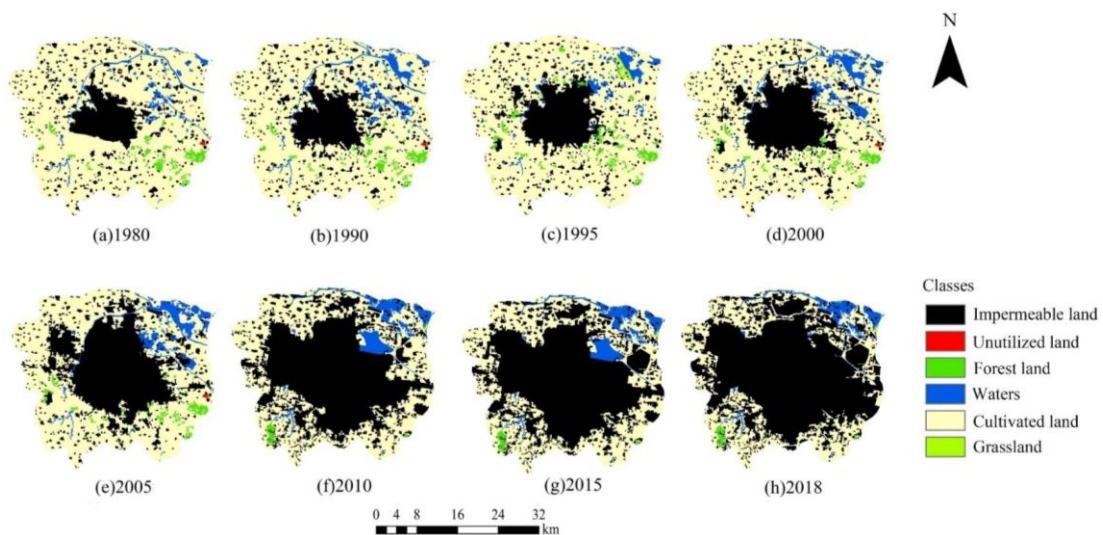
Table 2. Significance T-test of hypothetical mutation point

No.	n_1	n_2	T value of rainfall	T value of flood volume	$t_{\alpha/2}(a=0.01)$
12	11	12	1.530	3.452	2.831
24	12	27	-0.863	-4.310	2.715

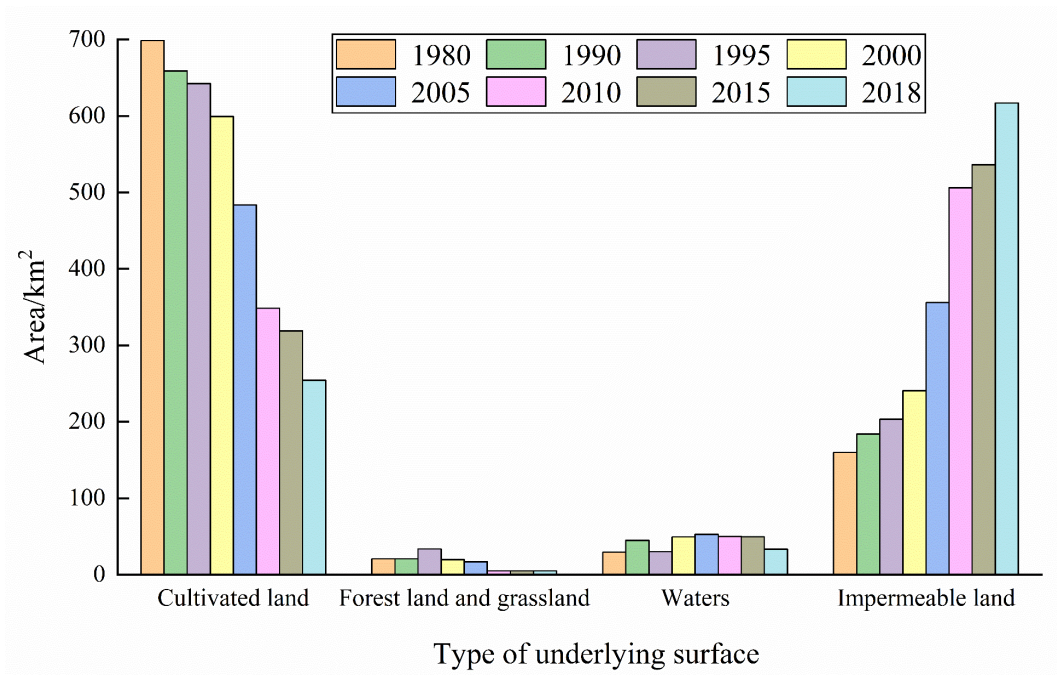
186 It can be seen from Table 2 that the flood volume decreases abruptly in the 12th rainstorm
187 flood and increases abruptly in the 24th rainstorm flood, the mutation of the latter is more
188 significant. Moreover, the rainfall does not change abruptly in these two rainstorm floods.
189 Therefore, the 12th and 24th rainstorm floods are mutation points of the relationship between
190 rainfall and flood volume, that is, the characteristics of runoff generation and concentration in
191 the study area change significantly in 1994 and 2005.

192 3.2 Determination of the Main Influencing Factors of Flood Volume

193 The land use/cover of study area is divided into 6 categories: cultivated land including dry
194 land and paddy field, forest land, grassland, waters, impermeable land and unutilized land
195 (shown in Figure 5), where the unutilized land mainly includes waste grassland, saline-alkali
196 land, swamp, sand, bare land, bare rock, etc. Furthermore, the area of different underlying
197 surface types is shown in Figure 6 (the unutilized land area is so small that it can be ignored).



198
199 **Figure 5. Land use distribution of study area in 1980, 1990, 1995, 2000, 2005, 2010,**
200 **2015 and 2018**



201

202

Figure 6. Area of different underlying surface types

203

204

205

206

207

208

209

210

211

From Figure 5 and Figure 6, it can be seen that the cultivated land area decreases continuously from 1980 to 2018, with the percentage decreasing from 76.8% to 28.0%, while the impermeable land area increases continuously, with the percentage increasing from 17.6% to 67.8%. Moreover, the area of forest and grassland accounts for 2.3% of the total area in 1990, increases to 3.7% in 1995, but then continues to decrease to 0.6 % in 2010. The water area basically remains unchanged from 2000 to 2015, with the percentage of 5.5%. The area changes of different underlying surface types in different periods are shown in Table 3.

Table 3. Area changes of different underlying surface types in different periods

(km²/a)

Period/Type	Cultivated land	Forest and grassland	Water	Impermeable land
1980~1990	-3.95	0.00	1.56	2.40
1990~1995	-3.29	2.56	-3.00	3.87

1995~2000	-8.64	-2.81	3.87	7.46
2000~2005	-23.15	-0.54	0.67	23.03
2005~2010	-27.04	-2.36	-0.53	30.06
2010~2015	-5.94	0.00	-0.09	6.03
2015~2018	-21.44	0.00	-5.48	26.92

212 Table 3 shows that both cultivated land area and impermeable land area change sharply in
 213 the two periods of 2000~2010 and 2015~2018, while change slightly from 1980 to 1995. The
 214 water area changes most sharply from 2015 to 2018 and changes slightly from 2000 to 2015,
 215 the area of forest and grassland changes sharply in the two periods of 1990~2000 and
 216 2005~2010, and basically remains unchanged in other periods.

217 Theoretically, the flood volume is affected by rainfall elements such as rainfall, rainfall
 218 duration and rainfall intensity. According to the selection principle of rainstorm floods and the
 219 analysis of the relationship between rainfall and flood volume, the rainfall is selected as the
 220 main influencing factor of flood volume among rainfall elements in this paper.

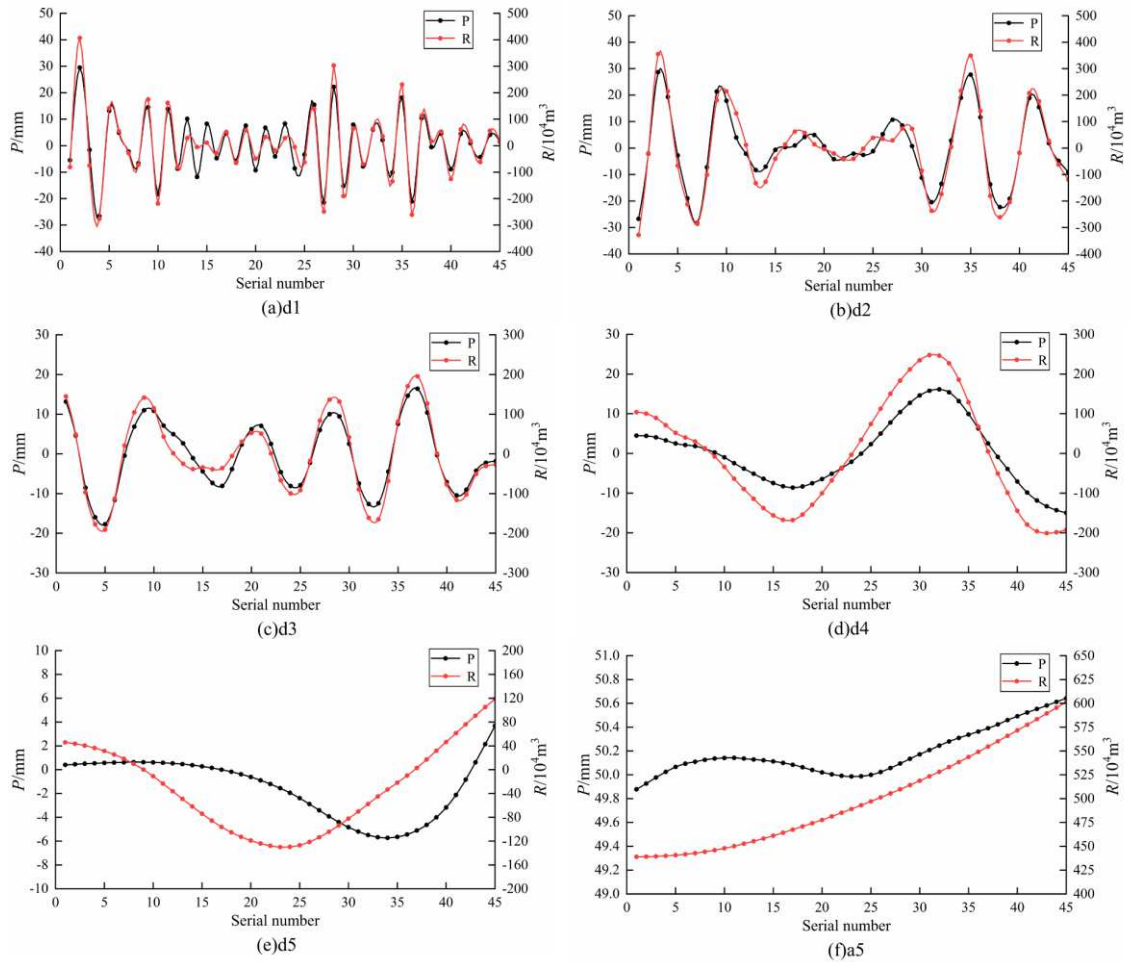
221 Furthermore, the increase of forest and grassland area or water area will lead to the
 222 decrease of runoff coefficient, reducing the flood volume generated by rainstorm of the same
 223 magnitude, while the increase of impermeable land area will lead to the opposite result.
 224 Therefore, according to the analysis of land/use change, it can be concluded the main reason
 225 for the mutation of the rainfall-flood volume relationship in 1994 is the change of forest and
 226 grassland area and water area under slight change of impermeable land area. Similarly, the main
 227 reason for the mutation of the rainfall-flood volume relationship in 2005 is the rapid

228 urbanization of Zhengzhou City and the rapid increase of impermeable land area after 2000.

229 The above conclusion is consistent with the previous study on the annual runoff coefficient
230 in the study area (Wang et al. 2017), that is, the underlying surface is the main driving factor
231 for urban rainstorm flood evolution. Therefore, the rainfall and underlying surface are the main
232 influencing factors of flood volume in the Jialu River Basin of Zhengzhou central urban area.

233 **3.3 Multiscale Attribution Analysis of Flood Volume**

234 In this paper, db6 wavelet (Daubechies wavelet of order 6) is selected to decompose the
235 rainfall sequence and flood volume sequence of the first 45 rainstorm floods, then five detail
236 components and one trend component are obtained respectively, that is d1, d2, d3, d4, d5 and
237 a5 (shown in Figure 7). The original sequence consists of these six component sequences, and
238 a5 reflects the overall change trend of the original sequence.



239

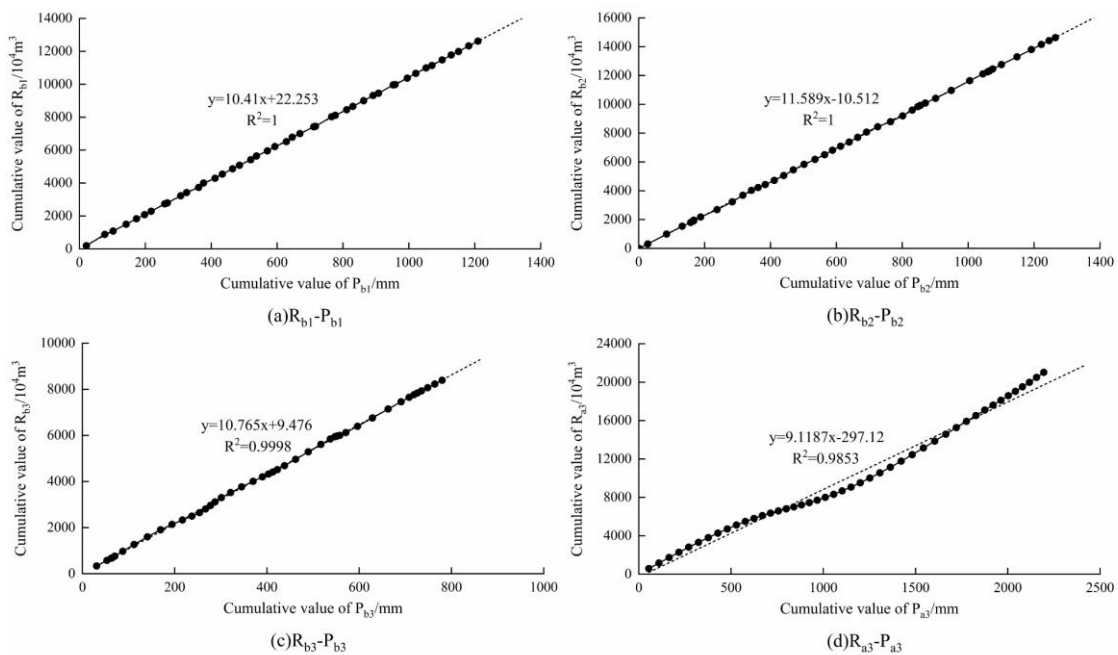
240 **Figure 7. Components of rainfall and flood volume for the first 45 rainstorm floods**

241 It can be seen from Figure.7 (a) that both P_{d1} and R_{d1} have fluctuation periods of quasi-
 242 2~4; (b) shows that both P_{d2} and R_{d2} have fluctuation periods of quasi-5~7; (c) shows that both
 243 P_{d3} and R_{d3} have fluctuation periods of quasi-8~12; (d) shows that R_{d4} has fluctuation period of
 244 quasi-26; (f) shows that the sequence of rainfall shows a slight change trend of increase-
 245 decrease-increase, while the sequence of flood volume shows a more obvious increase trend on
 246 the whole. In addition, the fluctuation trends of rainfall and flood volume are basically the same
 247 in d1, d2, d3 and d4.

248 In order to reasonably construct the multiscale prediction model to connect rainfall and
 249 flood volume at the micro level, the correlation coefficients between rainfall and flood volume

250 in each component are calculated as 0.957, 0.977, 0.974, 0.983, 0.319, 0.872, respectively. In
 251 other words, the rainfall and flood volume are positively correlated and well correlated in d1,
 252 d2, d3 and d4, while the correlation between the two variables is the worst in d5. Combining
 253 with Figure 7, d4, d5 and a5 components are superimposed to obtain the trend component a3 to
 254 improve the prediction accuracy of the model.

255 Since the decomposed sequences including d1, d2 and d3 have several negative values,
 256 the six data sequences are equivalently replaced for ease of calculation, that is, each item of
 257 original sequence subtracts the minimum value of the sequence to obtain new sequences
 258 including P_{b1} , P_{b2} , P_{b3} , R_{b1} , R_{b2} and R_{b3} . Then the double cumulative curves of P_{b1} - R_{b1} , P_{b2} - R_{b2} ,
 259 P_{b3} - R_{b3} and P_{a3} - R_{a3} are respectively constructed (shown in Figure 8).



260
 261 **Figure 8. Double cumulative curve of rainfall and flood volume in each component**

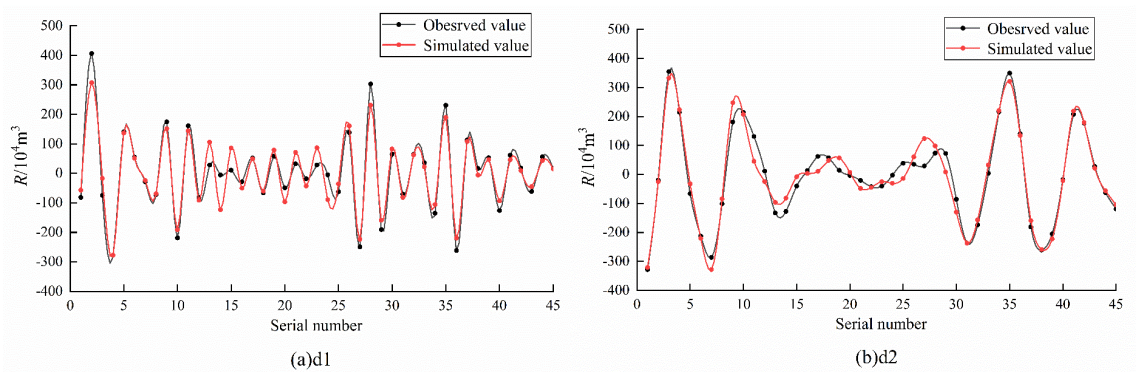
262 It can be seen from Figure 8(a), (b), (c) that the linear trend line basically coincides with
 263 the double cumulative curve, that is, there is a constant linear relationship between rainfall and

264 flood volume, while the change of underlying surface has little influence on flood volume in
 265 d1, d2 and d3. Moreover, Figure 8(d) shows that the slope of the double cumulative curve
 266 changes significantly in the 12th and 24th rainstorm floods, which is consistent with the analysis
 267 of the rainfall-flood volume relationship. Therefore, the impact of underlying surface on flood
 268 volume is mainly reflected in a3.

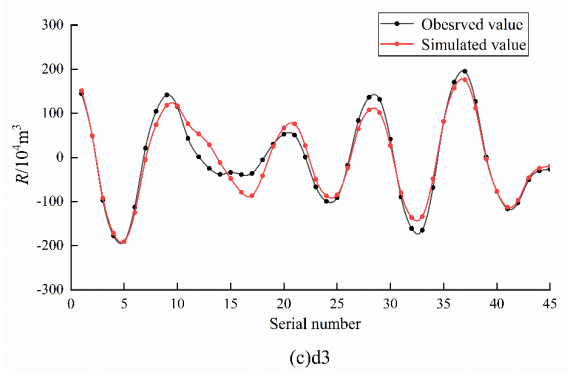
269 3.4 Construction of Prediction Model for Each Flood Volume Component

270 According to the multiscale attribution analysis of flood volume, the univariate model
 271 between flood volume and rainfall should be constructed for d1, d2 and d3 components of flood
 272 volume, while the multivariate model between flood volume, rainfall and various underlying
 273 surface areas should be constructed for a3 component of flood volume.

274 The cumulative linear regression models of $R_{b1}-P_{b1}$, $R_{b2}-P_{b2}$ and $R_{b3}-P_{b3}$ are respectively
 275 constructed, as shown in the trend line equation in Figure 8 (a)(b)(c), then the simulated value
 276 of R_{d1} , R_{d2} and R_{d3} can be obtained by restoring the simulation result. The comparison between
 277 the simulated and observed flood volume in d1, d2 and d3 components is shown in Figure 9.



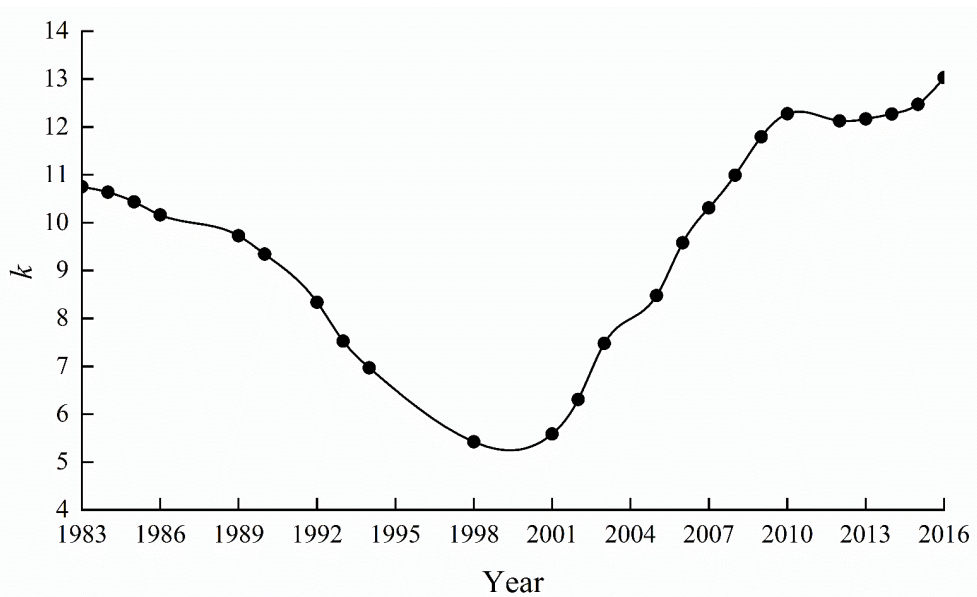
278



279

280 **Figure 9. Comparison between the simulated and observed flood volume in d1, d2 and**
 281 **d3 components**

282 The characteristics of runoff generation and concentration of the basin can be characterized
 283 by the rainfall-flood volume double cumulative curve slope, which is mainly affected by the
 284 underlying surface, thus, the slope of two adjacent points on the P_{a3} - R_{a3} double cumulative
 285 curve is calculated. Since the slopes of different rainstorm floods in the same year are not
 286 significantly different, their mean value is represented by k and taken as the slope in the given
 287 year, as shown in Figure 10 (where rainstorm floods are not screened out in some years such as
 288 1995 and 2004).



289

290

Figure 10. k value in each year

291 It can be seen from Figure 10 that the k value shows a decreasing trend from 1983 to 2000,
292 which is mainly influenced by the change of water area and forest and grassland area; the k
293 value shows an increasing trend after 2000, which is mainly influenced by the change of
294 impermeable land area. Therefore, the model between the k value and various underlying
295 surfaces area should be constructed before 2000 and after 2000, respectively. Moreover, the
296 sum of cultivated land area(S1), forest and grassland area(S2), water area(S3) and impermeable
297 land area(S4) is basically a constant value, thus, S1 is discarded to avoid strong collinearity
298 among the independent variables and up to other three variables are selected as independent
299 variables.

300 Taking the year after 2000 as an example, the correlation coefficients of S2, S3 and S4 are
301 0.53, -0.98 and -0.55 by combining Table 3 and assuming that S2, S3 and S4 change evenly in
302 the periods of 2000~2005, 2005~2010, 2010~2015 and 2015~2018, that is, there is a strong
303 collinearity among the three. Based on the analysis of land use/cover change, SPSS software is
304 used to respectively construct the linear regression model dependent on S4 for k value (Model
305 1), the ridge regression model dependent on S2 and S4 for k value (Model 2), the ridge
306 regression model dependent on S2, S3 and S4 for k value (Model 3). The equations of these
307 three models are as follows.

$$308 \quad k = (0.241S_4 - 1.782)/10 \quad (10)$$

$$309 \quad k = (-1.444S_2 + 0.088S_4 + 80.018)/10 \quad (11)$$

$$310 \quad k = (-1.404S_2 - 0.66S_3 + 0.086S_4 + 113.949)/10 \quad (12)$$

311 Similarly, for the year before 2000, the linear regression model dependent on S2 for k value

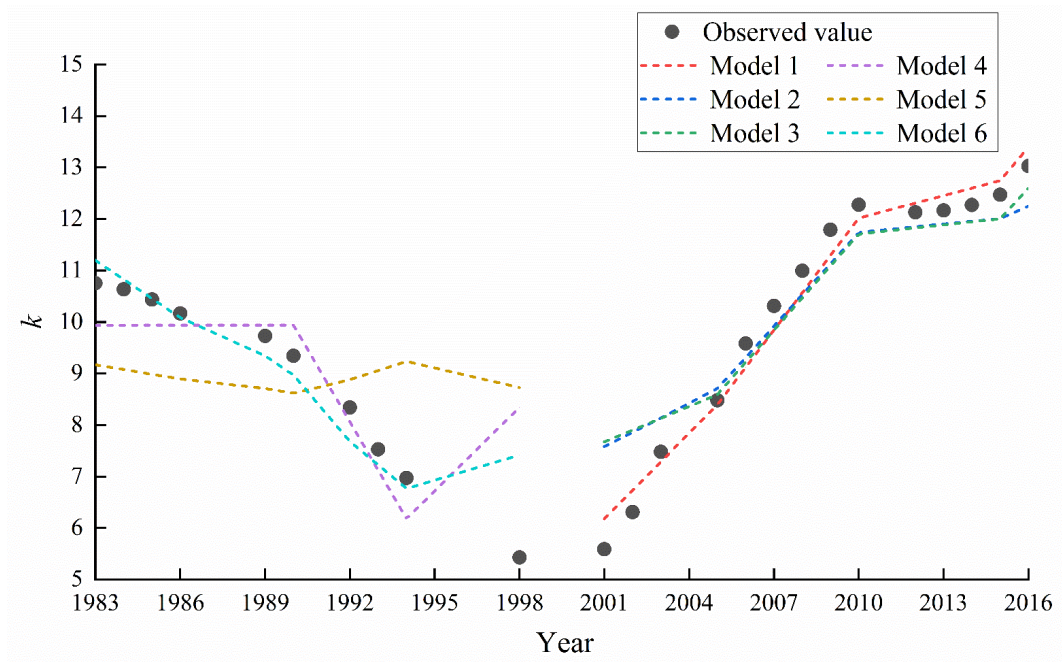
312 (Model 4), the linear regression model dependent on S3 for k value (Model 5) and the ridge
 313 regression model dependent on S2 and S3 for k value (Model 6) are respectively constructed.
 314 The equations of these three models are as follows.

$$315 \quad k = (-3.677S_2 + 176.36)/10 \quad (13)$$

$$316 \quad k = (-0.594S_3 + 112.01)/10 \quad (14)$$

$$317 \quad k = (-4.595S_2 - 2.386S_3 + 289.739)/10 \quad (15)$$

318 The simulation results of each model are shown in Figure 11 and the performance indexes
 319 of each model are shown in Table 4.



320

321 **Figure 11. The simulation results of each model**

321

322 **Table 4. The performance indexes of each model**

322

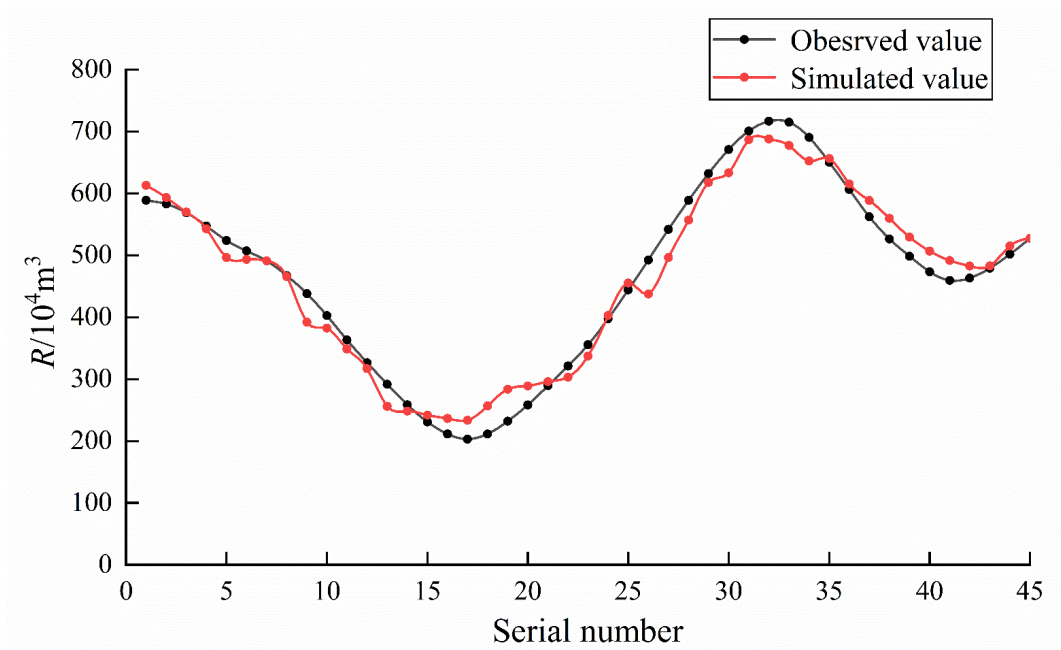
Index	Model 1	Model 2	Model 3	Model 4	Model 5	Model 6
<i>NSE</i>	0.976	0.886	0.881	0.616	0.013	0.827
<i>R²</i>	0.976	0.965	0.951	0.616	0.013	0.829

R_e	3.70%	7.81%	7.92%	10.36%	19.41%	6.64%
-------	-------	-------	-------	--------	--------	-------

323 From Figure 11 and Table 4, it can be seen that the Model 1 has the best simulation effect
 324 after 2000, while the Model 6 has the best simulation effect before 2000. Moreover, the Model
 325 6 has a poor simulation effect on the k value in 1998, which may be caused by uneven change
 326 of the underlying surface area from 1995 to 2000. All in all, the multivariate model for a_3
 327 component of flood volume before and after 2000 are shown in Eq. (16) and Eq. (17),
 328 respectively. The simulated flood volume component is shown in Figure 12.

329
$$R_{a_3} = (-4.595S_2 - 2.386S_3 + 289.739)P_{a_3}/10 \quad (16)$$

330
$$R_{a_3} = (0.241S_4 - 1.782)P_{a_3}/10 \quad (17)$$

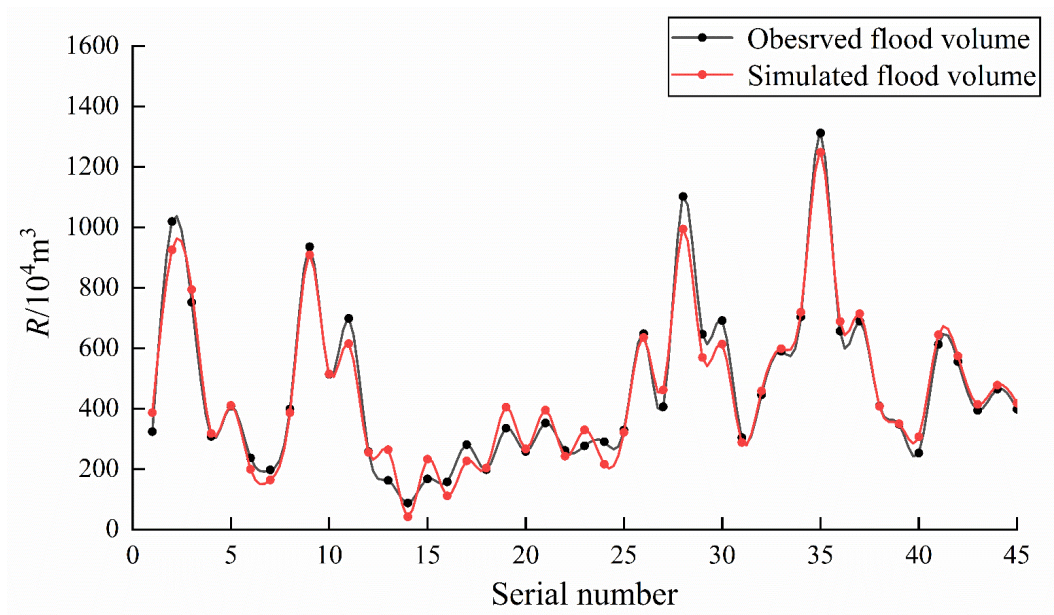


331
 332 **Figure 12. Comparison between the simulated and observed flood volume in a_3**
 333 **component**

334 **3.5 Effect Evaluation of the Multiscale-multivariate Prediction Model**

335 The multiscale-multivariate prediction model of urban rainstorm flood can be obtained by

336 superimposing all the component prediction models. The simulated flood volume of the first 45
 337 rainstorm floods is shown in Figure 13, where NSE , R^2 and R_e are 0.966, 0.964 and 10.80%,
 338 respectively. That is, the multiscale-multivariate prediction model has a good simulation effect
 339 on the flood volume of the first 45 rainstorm floods.



340

341 **Figure 13. The simulated flood volume of the first 45 rainstorm floods**

342 The rainfall of the 46th~50th rainstorm floods is decomposed and input into the model, in
 343 which the 46th~48th rainstorm floods occur in 2017 and the 49th~50th rainstorm floods occur
 344 in 2018. Then the flood volume can be predicted by combining the impermeable land area, the
 345 predicted flood volume of each rainstorm flood is shown in Table 5.

346 **Table 5. The predicted flood volume of the 46th~50th rainstorm floods**

No.	P_{d1}	P_{d2}	P_{d3}	P_{a3}	k	Predicted value	Observed value	Relative error
46	-3.76	-3.17	-2.63	40.26	14.04	461.2	439.9	4.84%

47	3.70	4.79	-4.28	41.49	14.04	630.6	647.0	-2.53%
48	-2.42	-3.38	-3.37	43.67	14.04	512.6	506.2	1.26%
49	-14.88	-10.38	-0.46	46.72	14.69	375.9	337.0	11.54%
50	24.28	3.80	4.02	50.70	14.69	1085.0	1080.6	0.41%

347 From Table 5, the relative errors between the predicted and observed flood volume of
348 46th~50th rainstorm floods are all less than 20%, indicating that the multiscale-multivariate
349 prediction model has a good prediction effect on flood volume.

350 4. Conclusion

351 Using wavelet analysis method, cumulative linear regression model and ridge regression
352 model, the multiscale-multivariate prediction model of urban rainstorm flood is constructed
353 which can not only reveal the relationship between flood volume and its influencing factors at
354 the micro level, but also predict flood volume at the micro and macro levels.

355 The analysis of rainfall-flood volume relationship and land use/cover change show that
356 the main influencing factors of flood volume are rainfall and underlying surface, and the change
357 of the underlying surface causes the mutation of characteristics of runoff generation and
358 confluence in 1994 and 2005.

359 At the micro level, the fluctuation trend and period of rainfall-flood volume in d1, d2 and
360 d3 are basically the same. The multiscale attribution analysis of flood volume shows that there
361 is a constant linear relationship between rainfall and flood volume in d1, d2 and d3, while the
362 change of underlying surface has little influence on flood volume. Moreover, the impact of
363 underlying surface on flood volume is mainly reflected in a3.

364 The multiscale-multivariate prediction model has a good simulation effect on the flood
365 volume of the first 45 rainstorm floods, NSE , R^2 and R_e are 0.966, 0.964 and 10.80%,
366 respectively. Moreover, the model also has a good prediction effect, and the relative errors
367 between the predicted and observed flood volume of the 46th~50th rainstorm floods are all less
368 than 20%.

369 In summary, the model has a good performance in exploring the overall impact of the
370 changing environment on urban rainstorm flood, quantifying the multiscale attribution
371 characteristics of flood volume, and predicting the flood volume. At the same time, the model
372 provides a new idea and method for flood prediction, and also provide an important basis for
373 urban flood management.

374

375 **Acknowledgments**

376 This study is supported by the Natural Sciences Foundation of Henan Province (No.
377 212300410404), the Open Grants of the State Key Laboratory of Severe Weather (No.
378 2021LASW-A15), Scientific and Technological Research Program of Henan Province (No.
379 192102310508).

380

381 **Availability of Data and Materials:** The raw/processed data required to reproduce these
382 findings cannot be shared at this time as the data also forms part of an ongoing study.

383

384 **Authors Contributions:** Conceptualization, Jinping Zhang, and Yuhao Wang; Methodology,

385 Jinping Zhang, and Yuhao Wang; Validation, Jinping Zhang, and Yuhao Wang; Writing-Original
386 Draft Preparation, Yuhao Wang; Writing-Review & Editing, Jinping Zhang, and Yuhao Wang;
387 Supervision, Jinping Zhang.

388 **Declarations**

389 **Ethical Approval:** The authors will comply with all academic norms by the journal of Water
390 Resources Management.

391 **Consent to Participate:** All authors agreed to join this research.

392 **Consent to Publish:** All authors agreed with the content and that all gave explicit consent to
393 submit.

394 **Competing Interests:** There is no conflict of interest

395 **References**

396 Bisht DS, Chatterjee C, Kalakoti S, Upadhyay P, Sahoo M, Panda A (2016) Modeling urban
397 floods and drainage using SWMM and MIKE URBAN: a case study. *Natural Hazards*
398 84(2):749-776.

399 Clark MP, Nijssen B, Lundquist JD, Kavetski D, Rupp DE, Woods RA, Freer JE, Gutmann ED,
400 Wood AW, Brekke LD, Arnold JR, Gochis DJ, Rasmussen RM (2015) A unified approach
401 for process-based hydrologic modeling: 1. Modeling concept. *Water Resources Research*
402 51(4):2498-2514.

403 Choi SH, Jung HY, Kim H (2019) Ridge Fuzzy Regression Model. *International Journal of*
404 *Fuzzy Systems* 21(7):2077-2090.

405 Chu HB, Wei JH, Li JY, Qiao Z, Cao JW (2017) Improved Medium- and Long-Term Runoff

406 Forecasting Using a Multimodel Approach in the Yellow River Headwaters Region Based
407 on Large-Scale and Local-Scale Climate Information. *Water* 9(8).

408 Gong YW, Li XN, Zhai DD, Yin DK, Song RN, Li JQ, Fang X, Yuan DH (2018) Influence of
409 Rainfall, Model Parameters and Routing Methods on Stormwater Modelling. *Water*
410 *Resources Management* 32(2):735-750.

411 Ho JY, Lee KT (2015) Grey Forecast Rainfall with Flow Updating Algorithm for Real-Time
412 Flood Forecasting. *Water* 7(5):1840-1865.

413 Jamali B, Lowe R, Bach PM, Urich C, Arnbjerg-Nielsen K, Deletic A (2018) A rapid urban
414 flood inundation and damage assessment model. *Journal of Hydrology* 564:1085-1098.

415 Li JK, Zhang B, Li YJ, Li HE (2018) Simulation of Rain Garden Effects in Urbanized Area
416 Based on Mike Flood. *Water* 10(7).

417 Liu JY, Zhang Q, Deng XY, Ci H, Chen XH (2016) Quantitative analysis the influences of
418 climate change and human activities on hydrological processes in Poyang Basin. *Journal*
419 *of Lake Sciences* 28(2):432-443.

420 Madarang KJ, Kang JH (2014) Evaluation of accuracy of linear regression models in predicting
421 urban stormwater discharge characteristics. *Journal of Environmental Sciences*
422 26(6):1313-1320.

423 Nigussie TA, Altunkaynak A (2019) Modeling the effect of urbanization on flood risk in
424 Ayamama Watershed, Istanbul, Turkey, using the MIKE 21 FM model. *Natural Hazards*
425 99(2):1031-1047.

426 Pathak P, Kalra A, Ahmad S, Bernardez M (2016) Wavelet-Aided Analysis to Estimate Seasonal

427 Variability and Dominant Periodicities in Temperature, Precipitation, and Streamflow in
428 the Midwestern United States. *Water Resources Management* 30(13):4649-4665.

429 Peng HQ, Liu Y, Wang HW, Ma LM (2015) Assessment of the service performance of drainage
430 system and transformation of pipeline network based on urban combined sewer system
431 model. *Environmental Science and Pollution Research* 22(20):15712-15721.

432 Rabiei MR, Arashi M, Farrokhi M (2019) Fuzzy ridge regression with fuzzy input and output.
433 *Soft Computing* 23(23):12189-12198.

434 Ren MF, Xu ZX, Pang B (2021) Driving mechanisms of urban floods under the changing
435 environment: case study in the Wenyu River basin. *Advances in Water Science* 32(3):345-
436 355.

437 Roushangar K, Nourani V, Alizadeh F (2018) A multiscale time-space approach to analyze and
438 categorize the precipitation fluctuation based on the wavelet transform and information
439 theory concept. *Hydrology Research* 49(3):724-743.

440 Seo Y, Kim S, Kisi O, Singh VP (2015) Daily water level forecasting using wavelet
441 decomposition and artificial intelligence techniques. *Journal of Hydrology* 520:224-243.

442 Shao DN, Liu GS (2018) Up-to-date urban rainstorm intensity formulas considering spatial
443 diversity in China. *Environmental Earth Sciences* 77(14).

444 Sun J, Zhang R, Qin L, Zhu HX, Huang Y, Xue YG, An SQ, Xie XC, Li AM (2017)
445 Genotoxicity and cytotoxicity reduction of the polluted urban river after ecological
446 restoration: a field-scale study of Jialu River in northern China. *Environmental Science
447 and Pollution Research* 24(7):6715-6723.

448 Taormina R, Chau K, Sivakumar B (2015) Neural network river forecasting through baseflow
449 separation and binary-coded swarm optimization. *Journal of Hydrology* 529:1788-1797.

450 Wang HL, Wu ZN, Sun RC (2017) Effect of Urbanization in Zhengzhou on River Hydrological
451 Process in Jialu River Watershed. *Science Technology and Engineering* 17(31):316-321.

452 Wang WC, Li WJ, Xu DM, Li QM (2019) Runoff prediction based on GM-BP model calibration
453 against Markov chain. *South-to-North Water Transfers and Water Science & Technology*
454 17(5):44-49.

455 Wu GZ, Wang C (2020) Research on runoff grey prediction based of improved fitting. *Yellow*
456 *River* 42(10):34-36&41.

457 Wu XS, Wang ZL, Guo SL, Liao WL, Zeng ZY, Chen XH (2017) Scenario-based projections
458 of future urban inundation within a coupled hydrodynamic model framework: A case study
459 in Dongguan City, China. *Journal of Hydrology* 547:428-442.

460 Xu LL, Liu JL, Jin CJ, Wang AZ, Guan DX, Wu JB, Yuan FH (2011) Baseflow separation
461 methods in hydrological process research: A review. *Chinese Journal of Applied Ecology*
462 22(11):3073-3080.

463 Wang FQ, Huo FL (2010) Summary of research on medium and long-term hydrological
464 forecasting methods. *Yellow River* 32(3):25-28.

465 Yan HF, Wang CH, Wen P (2008) Overview of Studies on Distributed Hydrological Model.
466 *Water Resources and Power* 26(6):1-4.

467 Yang MN, Xu YP, Pan GB, Han LF (2014) Impacts of Urbanization on Precipitation in Taihu
468 Lake Basin, China. *Journal of Hydrologic Engineering* 19(4):739-746.

469 Yaseen ZM, Jaafar O, Deo RC, Kisi O, Adamowski J, Quilty J, El-Shafie A (2016) Stream-flow
470 forecasting using extreme learning machines: A case study in a semi-arid region in Iraq.
471 Journal of Hydrology 542:603-614.

472 Zhang JY, Song XM, Wang GQ, He RM, Wang XJ (2014) Development and challenges of urban
473 hydrology in a changing environment: I : Hydrological response to urbanization.
474 Advances in Water Science 25(4):594-605.

475 Zhang KZ, Shen JQ, Han H, Jia YZ (2019) Urban River Health Analysis of the Jialu River in
476 Zhengzhou City Using the Improved Fuzzy Matter-Element Extension Model. Water 11(6).

477 Zhao SW, Liao J, Yu DL (2020) Model averaging estimator in ridge regression and its large
478 sample properties. Statistical Papers 61(4):1719-1739.

479 Zhou ZM, Liu JX, Guo W (2015) Comparison and Evaluation of Drainage Pattern and
480 Connectivity in Zhengzhou City. Yellow River 10:54-57.